Carbohydrate Polymers 102 (2014) 799–807

Contents lists available at ScienceDirect

Carbohydrate Polymers

journal homepage: www.elsevier.com/locate/carbpol

Crystalline and structural properties of acid-modified lotus rhizome C-type starch

Jinwen Cai[a,1], Canhui Cai[a,1], Jianmin Man[a], Yang Yang[a], Fengmin Zhang[b], Cunxu Wei[a,*]

[a] Key Laboratories of Crop Genetics and Physiology of the Jiangsu Province and Plant Functional Genomics of the Ministry of Education, Yangzhou University, Yangzhou 225009, China
[b] Testing Center, Yangzhou University, Yangzhou 225009, China

ARTICLE INFO

Article history:
Received 28 March 2013
Received in revised form 20 October 2013
Accepted 29 October 2013
Available online 6 November 2013

Keywords:
Lotus rhizome
C-type starch
Acid hydrolysis
Crystalline property
Structural property

ABSTRACT

The crystalline and structural properties of acid-modified C-type starch from lotus rhizomes were investigated using a combination of techniques. The degradation of granule during hydrolysis began from the end distant from the hilum and then propagated into the center of granule, accompanied by loss of birefringence. The crystallinity changed from C-type to A-type via C_A-type during hydrolysis. At the early stage of hydrolysis, the amylose content substantially reduced, the peak and conclusion gelatinization temperatures increased, and the enthalpy decreased. During hydrolysis, the double helix content gradually increased and the amorphous component decreased, the lamellar peak intensity firstly increased and then decreased accompanied by hydrolysis of amorphous and crystalline regions. This study elucidated that B-type allomorph was mainly arranged in the distal region of eccentric hilum, A-type allomorph was mainly located in the periphery of hilum end, and the center of granule was a mixed distribution of A- and B-type allomorphs.

1. Introduction

Starch consists of two main components: mainly linear amylose and highly branched amylopectin, and is stored as discrete semicrystalline granules in higher plants. Starch granules range from 1 to 100 μm in size and their structures are dependent on botanic origin (Blazek & Gilbert, 2011). Semicrystalline starch granules display a hierarchical structural periodicity, have a layered organization with alternating amorphous and semicrystalline radial growth rings of 120–400 nm thickness emanating from the hilum. The semicrystalline rings are formed by a lamellar structure of alternating amorphous and crystalline regions with a regular repeat distance of 9–10 nm. The crystalline regions are thought to be formed by double helices of amylopectin side chains packed laterally into a crystalline lattice (Blazek & Gilbert, 2011).

There are three types of starches known as A-, B- and C-type according to their X-ray powder diffraction (XRD) patterns (Cheetham & Tao, 1998). The A-type starches are usually found in normal cereal seeds, B-type starches exist in tubers and high-amylose cereal seeds, and C-type starches occur in rhizomes and legume seeds (Bogracheva, Morris, Ring, & Hedley, 1998; Cheetham & Tao, 1998; Wang, Yu, Zhu, Yu, & Jin, 2009). A- and B-type starches contain A- and B-type crystalline structure, respectively. C-type starch is a mixture of A- and B-type crystalline structures (Bogracheva et al., 1998; Buléon, Gérard, Riekel, Vuong, & Chanzy, 1998; Wang et al., 2009). The A-type crystalline structure is formed by amylopectin with short lateral chains and closed branching points, and the packing of the double helices is relatively compact with low water content. The B-type crystalline structure is usually formed by amylopectin with long side chains and distant branching points, and has a more open structure containing a central water-filled cavity surrounded by six double helices (Blazek & Gilbert, 2011; Cheetham & Tao, 1998).

Many researchers have reported A- and B-type starches, however, there is little information on C-type starch. C-type starch contains A- and B-type allomorphs within the same granule (Bogracheva et al., 1998; Buléon et al., 1998; Wang et al., 2009). The arrangements of A- and B-type allomorphs in C-type starch granule affect the properties of starch, and are worth investigating (Bogracheva et al., 1998). In smooth pea starch, the most well-known example of C-type starch, the center of the starch granule consists mainly of the B-type allomorph whereas the A-type allomorph is located toward the outside of the granule (Bogracheva et al., 1998; Buléon et al., 1998). For C-type starch granules of Chinese yam, A- and B-type allomorphs coexist in individual granule,

Abbreviations: ATR-FTIR, attenuated total reflectance-Fourier transform infrared; ^{13}C CP/MAS NMR, ^{13}C cross-polarization magic-angle spinning nuclear magnetic resonance; DSC, differential scanning calorimetry; SAXS, small-angle X-ray scattering; SEM, scanning electron microscope; XRD, X-ray powder diffraction.

* Corresponding author at: College of Bioscience and Biotechnology, Yangzhou University, Yangzhou 225009, China. Tel.: +86 514 87997217.
E-mail address: cxwei@yzu.edu.cn (C. Wei).

[1] These authors contributed equally to this work.

0144-8617/$ – see front matter © 2013 Elsevier Ltd. All rights reserved.
http://dx.doi.org/10.1016/j.carbpol.2013.10.088

the B-type allomorph locates at the central part of the granule and is surrounded by the A-type allomorph at the granule periphery (Wang et al., 2009). In high-amylose rice TRS C-type starch, the A-type allomorph is located around the amorphous region and is surrounded by the B-type allomorph located in the peripheral region of the subgranules and the surrounding band of the starch granule (Wei, Qin, et al., 2010). The other allomorph distribution patterns of C-type starches have not been reported but there have been two above reported patterns.

Lotus (*Nelumbo nucifera* Gaertn.), an aquatic perennial from family Nelumbonaceae, is an important economic plant which is widely cultivated in China, India, Japan and Australia. Lotus rhizome is rich in C-type starch. There have been some studies about the physicochemical properties of native lotus rhizome starch (Lin et al., 2006; Man, Cai, et al., 2012). However, the distributions of A- and B-type allomorphs in lotus C-type starch granule remain unclear.

Acid modification does not change the crystalline characteristics of A- and B-type starches, but can change the morphological and structural properties of starch (Wang & Wang, 2001). Acid treatment is often used to investigate the allomorph distribution and structural properties of C-type starches (Wang, Yu, Yu, Chen, & Pang, 2007; Wang et al., 2009; Wei, Qin, et al., 2010). In this study, the crystalline and structural properties of acid-modified lotus rhizome C-type starch were investigated using XRD, ^{13}C cross-polarization magic-angle spinning nuclear magnetic resonance (^{13}C CP/MAS NMR), attenuated total reflectance-Fourier transform infrared (ATR-FTIR) and small-angle X-ray scattering (SAXS) in combination with differential scanning calorimetry (DSC), scanning electron microscope (SEM) and polarized microscope. This study would add to our understanding of allomorph distribution and property of C-type starch, and be helpful in the application of lotus rhizome starch in food and nonfood industries.

2. Materials and methods

2.1. Starch

Freshly harvested rhizomes of lotus (*N. nucifera* Gaertn.) were obtained from a local natural food market (Yangzhou City, China). Native starch was isolated from peeled rhizomes following the method described by Man, Cai, et al. (2012).

2.2. Acid hydrolysis

The acid-modified starch was prepared according to the methods of Li, Corke, and Beta (2007) with some modifications. Triplicate samples of isolated native starch (2 g) were each suspended in 100 ml of 2.2 M HCl solution. The starch slurries were placed in a water bath at 40 °C for 4, 8, 12, 16, 24, 36, 48, 72, 96 h and gently shaken 3 times by hand every day to resuspend the sedimented granules. After hydrolysis, undissolved residues were quickly obtained by centrifugation (5000 × *g*, 10 min), and the supernatant was used for measurement of the solubilized carbohydrates to quantify the hydrolysis degree by the anthrone-H_2SO_4 method. The residues were subsequently washed four times with double-distilled water and twice with anhydrous ethanol, and then dried at 40 °C for 2 days. The dried starches were ground into powders in a mortar with pestle and passed through a 100-mesh sieve for structural analyses.

2.3. Light microscopy

For in situ viewing the hydrolysis process, starch suspension was prepared by suspending about 10 mg starch in 1.0 ml of 2.2 M HCl by using a vortex mixer. The suspension was transferred onto a slide, covered with a coverslip, and sealed with nail polish to prevent moisture loss during heating. The sealed specimen was then mounted on a Kitazato hot stage apparatus at 40 °C and observed under a long focus M Plan Semi Apochromat objective using an Olympus BX53 polarized microscope during hydrolysis. The behaviors of more than fifty starch granules during hydrolysis were in situ viewed with a 50× objective under normal and polarized light, and photographed using an Olympus DP72 CCD camera. For acid-modified starch in water bath, starch slurries was directly placed on the microscope slide and covered with a coverslip. The starch granule shape and birefringence were viewed and photographed.

2.4. SEM observation

Starch was suspended in anhydrous ethanol. One drop of the starch–ethanol suspension was applied to an aluminum stub using double-sided adhesive tape. The starch was coated with gold before viewing with an environmental SEM (Philips XL-30).

2.5. XRD analysis

XRD analysis of starch was carried out on an XRD (D8, Bruker, Germany), and the relative crystal degree was measured following the method described by Wei, Qin, et al. (2010).

2.6. ATR-FTIR analysis

ATR-FTIR analysis of starch was carried out on a Varian 7 000 FTIR spectrometer with a DTGS detector equipped with an ATR single-reflectance cell containing a germanium crystal (45° incidence-angle) (PIKE Technologies, USA) as previously described (Wei, Xu, et al., 2010). Spectrum was corrected by a baseline in the region from 1200 to 800 cm^{-1} before deconvolution was applied using Resolutions Pro. The assumed line shape was Lorentzian with a half-width of 19 cm^{-1} and a resolution enhancement factor of 1.9. Intensity measurements at 1045, 1022 and 995 cm^{-1} were performed on the deconvoluted spectrum by recording the height of the absorbance bands from the baseline using Adobe Photoshop 7.0 image software.

2.7. ^{13}C CP/MAS NMR analysis

High-resolution ^{13}C CP/MAS NMR analysis of starch was carried out at B_0 = 9.4 T on a Bruker AVANCE III 400 WB spectrometer as described previously by Wei, Xu, et al. (2010). The amorphous starch was prepared by gelatinizing starch following the method of Atichokudomchai, Varavinit, and Chinachoti (2004). The quantitative analyses of double helix, single helix and amorphous conformational features within starch were carried out according to the method described by Tan, Flanagan, Halley, Whittaker, and Gidley (2007). The analysis of the NMR spectra involved the decomposition of the spectra into amorphous and ordered subspectra. The spectrum of amorphous starch was matched to the intensity of native or acid-modified starch at 84 ppm and was subtracted to produce the ordered subspectrum. The areas of the amorphous and ordered subspectra relative to the total area of spectrum at C1 region yielded the percentage of amorphous and ordered components, respectively. The ordered subspectrum was peak fitted by using PeakFit® version 4.12, and yielded four individual peaks at 99.5, 100.5, 101.5 and about 103 ppm for C1 region. The peak at 103 ppm was coincident with the C1 chemical shift of the single helix V-type conformation, and the peaks at 99.5, 100.5 and 101.5 ppm were double helix components. Comparing the areas of single helix and double helix peaks at C1 region in the ordered subspectrum, the relative proportions of single helix and double helix within the starch were obtained.

2.8. SAXS analysis

SAXS measurement of starch was performed according to the method of Yuryev et al. (2004) with some modifications. Powders of starches were dispersed in an excess of distilled water to form slurries. SAXS measurement was obtained using a Bruker NanoStar SAXS instrument equipped with Vantec 2000 detector and pin-hole collimation for point focus geometry. The X-ray source was a copper rotating anode (0.1 mm filament) operating at 50 kV and 30 W, fitted with cross coupled Göbel mirrors, resulting in Cu Kα radiation wavelength of 1.5418 Å. The optics and sample chamber were under vacuum to minimize air scattering. During X-ray exposure, the starch slurries were kept in sealed cells to prevent dehydration. SAXS datasets were analyzed using DIFFRAC^{plus} NanoFit software. Parameters of the SAXS spectrum were determined according to the simple graphical method (Yuryev et al., 2004).

2.9. Amylose content determination

Amylose content of starch was determined according to the iodine adsorption method of Konik-Rose et al. (2007). The experiments were performed in triplicate.

2.10. DSC analysis

Thermal property of starch was measured using a DSC (200-F3, NETZSCH, Germany) as described previously by Wei et al. (2011). Starch (5 mg) was precisely weighed and mixed with 3 times (15 μl) deionized water. The mixture was sealed in an aluminum pan overnight at 4 °C. After equilibrating for 1 h at room temperature, the starch sample was then heated from 30 to 110 °C at a rate of 10 °C/min. The experiments were performed in duplicate.

2.11. Statistical analysis

Analysis of variance (ANOVA) by Tukey's test ($p < 0.05$) was evaluated using the SPSS 16.0 Statistical Software Program.

3. Results and discussion

3.1. Acid hydrolysis of native starch

Insoluble residues after acid hydrolysis of granular starches are referred to as lintnerised starch in the case of hydrolysis with 2.2 M HCl at elevated temperatures (30–40 °C) (Chung & Lai, 2006). Generally, starches are hydrolyzed by 2.2 M HCl at 35 °C (Wang et al., 2007, 2009; Wei, Xu, et al., 2010). Increasing the hydrolysis temperature obviously shortens the time needed for the same degree of starch hydrolysis (Chung & Lai, 2006). In order to in situ view the hydrolysis process of starch for a short time, lotus starch was hydrolyzed with 2.2 M HCl at 40 °C instead of 35 °C in this study. The hydrolysis degrees of lotus native starch by HCl for different time are presented in Fig. 1. Two phases were distinguished in the acid hydrolysis of starch as a function of time. The initial rapid hydrolysis phase occurred from 0 to 48 h, and then later slower hydrolysis phase after 48 h. The two phases of hydrolysis profile were comparable with those reported in the literature (Jacobs, Eerlingen, Rouseu, Colonna, & Delcour, 1998; Man, Cai, et al., 2012). The initial rapid hydrolysis phase was mainly attributed to the hydrolysis of amorphous starch domains, and the later slower hydrolysis phase corresponded to the hydrolysis of the crystalline starch domains.

3.2. Light microscope observation of acid-modified starch

The behaviors of starch granules during hydrolysis were in situ viewed by observing granular shape and birefringence using polarized microscope with normal and polarized light (Fig. 2A). Lotus native starch had the eccentric hilum at one end of granule, was birefringent and showed the characteristic "Maltese cross" pattern under polarized light (Fig. 2A), which was in agreement with the report of Man, Cai, et al. (2012). The shape and birefringence of acid-modified starch was similar to that of native starch for 4–12 h of hydrolysis (data not shown). At 16 h of hydrolysis, growth rings were clearly observed, and a tunnel with low contrast began to form from the end opposite to the hilum. The tunnel gradually widened and propagated to the hilum, and growth rings became clearer at 24 and 36 h of hydrolysis. After 48 h of hydrolysis, the growth rings gradually became unclear with increasing hydrolysis time, and the central tunnel was clearly observed. Native starch granule has a layered organization with alternating amorphous and semicrystalline growth rings (Man, Cai, et al., 2012; Wang et al., 2009). The amorphous growth rings were firstly hydrolyzed at the early stage of hydrolysis, which resulted in the appearance of clear semicrystalline growth rings. After 48 h of hydrolysis, the hydrolysis of the crystalline starch domains decreased the contrast of growth rings. The morphology changes were in agreement with the two phases of starch lintnerisation profiles (Fig. 1; Jacobs et al., 1998; Man, Cai, et al., 2012).

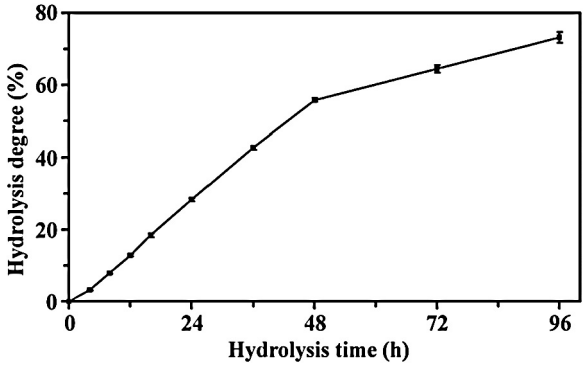

Fig. 1. Hydrolysis degree of starch as a function of time.

Birefringence pattern indicates a radial alignment of crystallites within starch granules, and the loss of birefringence suggests the loss of crystallites (Pérez, Baldwin, & Gallant, 2009). Before 36 h of hydrolysis, the birefringence of acid-modified lotus starch was similar to that of native starch. After 36 h of hydrolysis, the birefringence began to gradually vanish from the end opposite to the hilum, then to the central tunnel region. The periphery of hilum showed birefringence at 96 h of hydrolysis (Fig. 2A). The morphology and birefringence changes of starch residues hydrolyzed in water bath were similar to that on hot stage, and the data were not shown.

According to light microscope observation of acid-modified starches on hot stage and in water bath, lotus starch granule could be categorized into three parts. The first part was the region located on the end of granule opposite to the hilum, which firstly lost the birefringence. The second part was the central tunnel area, which had the weak birefringence at late stage of hydrolysis. The third part was the periphery of hilum, which had clear birefringence even when the first and second parts had lost birefringence. This result agreed with the findings of Lin et al. (2006) that the partially digested lotus starch granule by α-amylase could be categorized into three parts under the light microscope.

3.3. SEM observation of acid-modified starch

SEM micrographs of lotus native and acid-modified starch granules are displayed in Fig. 2B. Most of the native starch granules were elongated in shape with large size or oval with relative smaller size. The surface of granules was smooth. Some dents were observed

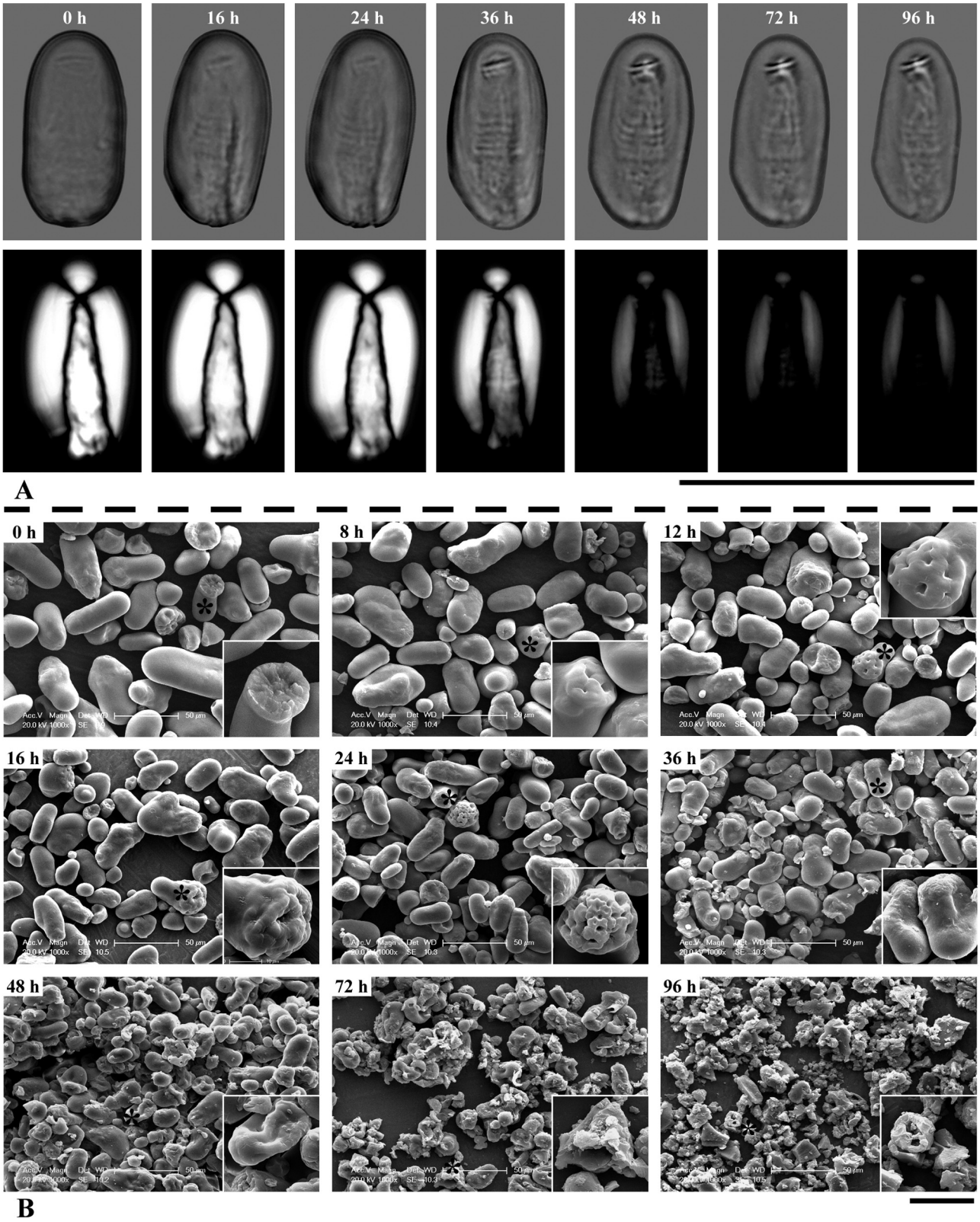

Fig. 2. In situ shape and birefringence changes of starch granule under normal light and polarized light during hydrolysis (A) and SEM micrographs of acid-modified starches (B). Inserts were the asterisk regions at high magnification. Scale bar = 50 μm.

at the one end of the granule opposite to the hilum location. The morphological characters of lotus native starch granules were in agreement with the previous reports (Lin et al., 2006; Man, Cai, et al., 2012). When the starch was subjected to 4 h of acid hydrolysis, no obvious changes occurred from the SEM photographs (data not shown). After 8 h of hydrolysis, some pores began to appear on the one end of granule opposite to the hilum. The quantity and size of pores gradually increased with increasing hydrolysis time.

When starch granules were subjected to 36 h of acid hydrolysis, some indentations were observed on granule surface opposite to the hilum, however, the hilum end was intact. This phenomenon became more obvious at 48 h of hydrolysis. At 72 h of hydrolysis, the central cavity was clearly visible within some cracked starch granules, indicating that the center of the granules was essentially hollow. From the evidence provided by SEM, the HCl firstly hydrolyzed the granule from the end opposite to the hilum location, then degraded the center of granule to form a hollow tunnel. The periphery of granule, especially around the hilum was resistant to acid hydrolysis. This result was in agreement with the light microscope observation (Fig. 2A). At the early stage of acid hydrolysis, the particle size of acid-modified starch did not change significantly compared with native starch. However, the average particle size significantly reduced after 36 h of hydrolysis. At 96 h of hydrolysis, most of the acid-modified starch granule ruptured and broke into pieces. The size changes of acid-modified starch agreed with that of acid-modified Chinese yam starch (Wang et al., 2007).

3.4. XRD spectra of acid-modified starch

C-type starches contain different proportions of A- and B-type crystalline structures, and can be further classified to C_A-type (closer to A-type), C-type and C_B-type (closer to B-type) starch according to XRD patterns. The typical C-type starch shows strong diffraction peaks at about 17° and 23° 2θ, and a few small peaks at around 5.6° and 15° 2θ. C_A-type starch shows a shoulder peak at about 18° 2θ, which is indicative of the A-type allomorph. C_B-type starch shows two shoulder peaks at about 22° and 24° 2θ, which are indicative of the B-type allomorph (Cheetham & Tao, 1998). XRD spectra of lotus native and acid-modified starches are shown in Fig. 3A. Native starch showed C-type crystalline structure, and was in agreement with the previous report (Lin et al., 2006; Man, Cai, et al., 2012). There were three remarkable differences in the XRD patterns of acid-modified starches during hydrolysis. First, the intensity of the peak at 5.6° 2θ was found to decrease and disappear with increasing hydrolysis time. Second, the peak at 18° 2θ began to appear and its intensity increased during hydrolysis. The peak at around 17° 2θ became a doublet at around 17° and 18° 2θ, which was the typical A-type characteristic. The last notable difference was that the peaks at 15° and 23° 2θ gradually sharpened during hydrolysis. The above three differences in XRD patterns showed the disappearance of the characteristic B-type diffraction peak and the development of typical A-type diffraction peak, which indicated that lotus starch crystallinity changed from typical C-type to A-type via C_A-type during hydrolysis. This result was in agreement with that the crystalline structure of C-type pea and Chinese yam starches changed from C-type to A-type during acid hydrolysis (Wang et al., 2007, 2009; Wang, Blazek, Gilbert, & Copeland, 2012). Acid modification does not change the crystalline characteristics of A-type and B-type starches (Wang & Wang, 2001). The crystalline type change of acid-modified lotus C-type starch revealed that the B-type allomorph in C-type starch was firstly degraded or degraded faster than A-type allomorph in the process of acid hydrolysis (Wang et al., 2007, 2009, 2012).

The relative crystal degrees of acid-modified starches calculated from the ratio of diffraction peak area and total diffraction area are given in Fig. 3A. The relative crystal degree did not show significant change before 16 h of hydrolysis, then gradually increased with increasing the hydrolysis time. The changes of crystal degrees were comparable with those reported in the literature (Wang et al., 2007, 2012), and showed that amorphous component of starch was hydrolyzed faster than the crystalline component.

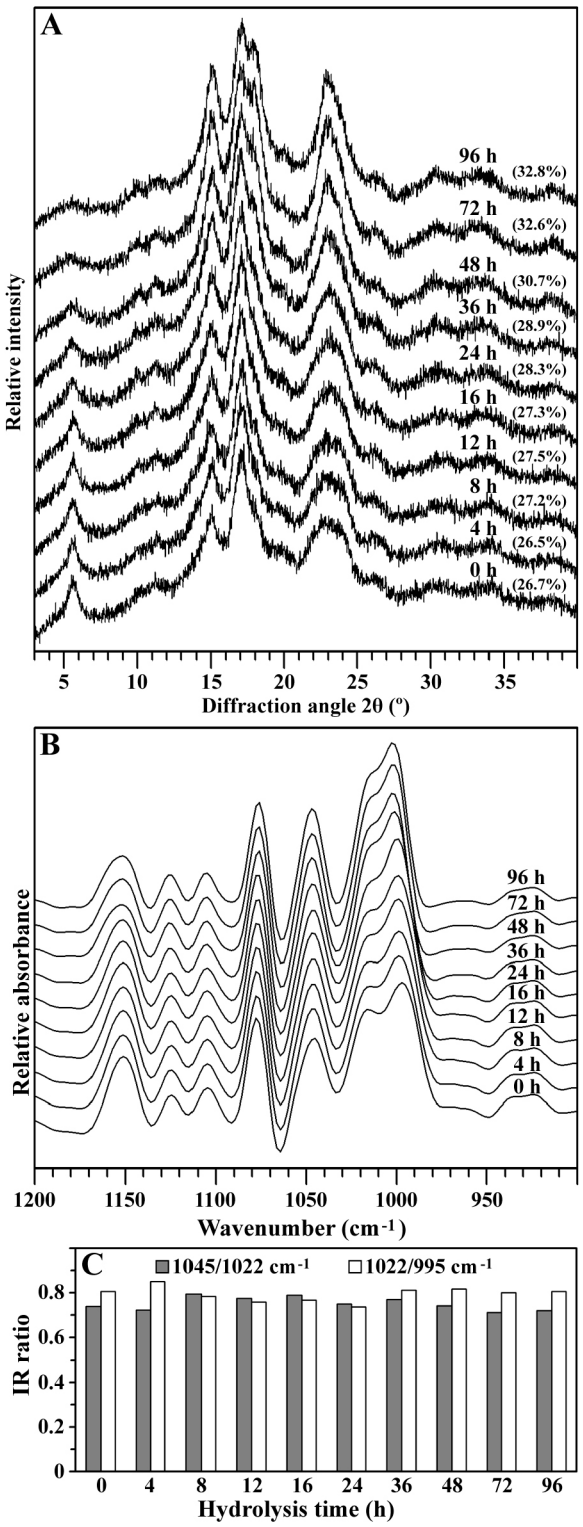

Fig. 3. XRD patterns (A), ATR-FTIR deconvoluted spectra (B) and the absorbance ratios (C) of acid-modified starches. The relative crystal degrees were given in parentheses of (A).

3.5. ATR-FTIR spectra of acid-modified starch

The development of sampling devices like ATR-FTIR combined with procedures for spectrum deconvolution provides opportunities for the study of starch structure (Sevenou, Hill, Farhat, & Mitchell, 2002). Though it has been proposed that ATR-FTIR is not

related with XRD and unable to differentiate starch long-range order characteristics and polymorphism, the spectrum variation of starch is interpreted in terms of the level of short-range order structure present on the edge of starch granules. The absorbance band intensities at 1045, 1022, and 995 cm^{-1} are sensitive to changes in starch conformation. The bands at 1045 and 1022 cm^{-1} have been linked with order/crystallinity and amorphous regions in starch, respectively. The intensity ratios of 1045/1022 and 1022/995 cm^{-1} are useful as a convenient index of FTIR data in comparisons with other measures of starch conformation (Htoon et al., 2009; Sevenou et al., 2002).

The deconvoluted ATR-FTIR spectra in the region 1200–900 cm^{-1} of lotus acid-modified starches are presented in Fig. 3B. The ratios for 1045/1022 and 1022/995 cm^{-1} were calculated as shown in Fig. 3C. For native starch, the starches with same crystal type always show the similar FTIR spectra, the band at 1022 cm^{-1} is more pronounced in A-type starch than in B-type or C-type starches (Sevenou et al., 2002). The ATR-FTIR spectrum of lotus native starch was similar to those of other native C-type starch (Sevenou et al., 2002; Wei, Xu, et al., 2010). Though the spectra of acid-modified lotus starches showed slightly changes, the ratios for 1045/1022 and 1022/995 cm^{-1} were similar during hydrolysis (Fig. 3B and C). This result was not in agreement with that of acid-modified rice starch (Wei, Qin, et al., 2010). According to the theory of ATR, the penetration depth is related to the wavelength. Polysaccharides, such as starch, absorb in the region 1200–800 cm^{-1}, that is, at wavelengths between about 8 and 12 μm. In this region, the average penetration depth is about 2 μm (Sevenou et al., 2002). The average particle size was 26.6 μm and 3.9 μm for lotus rhizome starch and rice starch, respectively (Man, Cai, et al., 2012; Wei, Qin, et al., 2010). The result of acid-modified rice starch corresponded to the short-range ordered structure of whole granule, however, that of acid-modified lotus starch corresponded to the short-range ordered structure of the external 2 μm thick region, which was resistant to hydrolysis (Fig. 2).

3.6. ^{13}C CP/MAS NMR spectra of acid-modified starch

The ^{13}C CP/MAS NMR has been employed in examining the molecular organization at short-range distance. The different crystalline polymorphic forms of starch as well as amorphous starch have been reported to exhibit different ^{13}C NMR spectral features (Tan et al., 2007). Most of the resonances cannot be distinguished or have not been assigned among the A-, B- and C-type starches, but the C1 resonance contains information both on the crystalline nature as well as the noncrystalline (but rigid) chains. The multiplicity of the C1 resonance corresponds to the packing type of starch granule. The C1 peak of spectrum is a triplet for A-type starch, and a doublet for B-type starch (Atichokudomchai et al., 2004). For C-type starch, the C1 spectrum shows a mixed pattern of both A- and B-type, and depends on the relative proportions of A- and B-type allomorphs in the sample (Bogracheva, Wang, & Hedley, 2001).

Fig. 4A and a compare the ^{13}C CP/MAS NMR original spectra of lotus native and acid-modified starches. Assignments of the ^{13}C CP/MAS NMR resonance are consistent with literature data (Atichokudomchai et al., 2004; Bogracheva et al., 2001). Signals at 94–105 and 58–65 ppm are attributed to C1 and C6 in hexapyranoses, respectively; the overlapping signal around 68–78 ppm is associated with C2, C3 and C5; and the broad resonance at 82 ppm appears from the amorphous domains for C4. The two broad shoulders that appear at 103 and 95 ppm can arise from the amorphous domains for C1. The C1 resonances of lotus native starch showed inconspicuous doublet or triplet, indicating the character of C-type starch, which was in agreement with the result of XRD. The C1 resonance of acid-modified starch gradually became triplet at 99.5, 100.5 and 101.5 ppm (Fig. 4a), which indicated that B-type

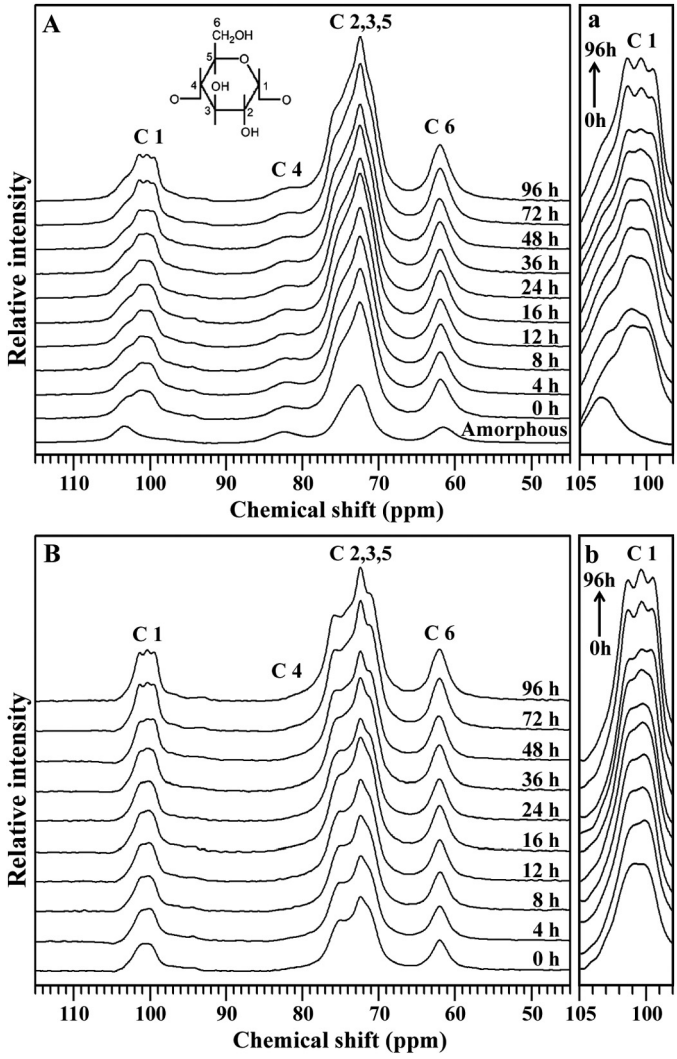

Fig. 4. ^{13}C CP/MAS NMR original spectra (A and a) and ordered subspectra (B and b) of acid-modified starches.

allomorph in the C-type starch was hydrolyzed faster than the A-type allomorph, and starch became A-type crystallinity during hydrolysis. This result was in agreement with that of acid-modified Chinese yam starch (Wang et al., 2009).

Fig. 4B and b are the ordered subspectra of acid-modified starches, which involves the subtraction of a standard amorphous starch spectrum from the test spectrum until there is no residual intensity at 84 ppm (a region of the spectrum with intensity due solely to amorphous conformations) (Tan et al., 2007). The ordered subspectra were similar to the origin spectra, but they had more clear crystalline peaks of C1 resonances than the origin spectra. The C1 resonances gradually changed from inconspicuous triplet or doublet to clear triplet with increasing hydrolysis time, indicating that C-type starch gradually became to A-type starch. The ordered subspectra at C1 region were peak fitted by using peakfit (data not shown). The results from quantitative analysis of the proportion of single helix, double helix, and amorphous component according to the method described by Tan et al. (2007) are summarized in Table 1. The gradual increase in double helix component and decrease in amorphous and single helix contents were observed during hydrolysis. This result was in agreement with that of acid-modified rice starch (Man, Qin, et al., 2012).

Table 1
The relative proportions of single helix, double helix and amorphous conformation and the SAXS parameters of acid-modified starches.

Acid-modified starches (h)	Relative proportion (%)[a]			SAXS parameters[b]			
	Amorphous	Single helix	Double helix	I_{max} (counts)	S_{max} ($Å^{-1}$)	ΔS ($Å^{-1}$)	D (nm)
0	44.7	3.5	51.8	452	0.061	0.018	10.3
4	41.9	3.2	54.9	820	0.061	0.017	10.3
8	39.0	2.9	58.1	931	0.061	0.017	10.3
12	37.2	2.5	60.3	984	0.061	0.017	10.3
16	36.5	2.3	61.2	859	0.061	0.016	10.3
24	36.3	1.9	61.7	590	0.061	0.015	10.3
36	35.4	1.2	63.4	243	–[c]	0.015	–
48	35.1	0.9	64.0	79	–	0.013	–
72	32.3	0.7	67.0	–	–	–	–
96	30.6	0.6	68.8	–	–	–	–

[a] The relative proportion was calculated from the ^{13}C CP/MAS NMR ordered subspectra following the method of Tan et al. (2007).
[b] The parameters were determined as shown in Fig. 5A. I_{max}, peak intensity; S_{max}, maximum peak position; ΔS, peak width at half maximum.
[c] Data were not detected.

Table 2
Amylose contents (AC) and DSC parameters of acid-modified starches [a]

Acid-modified starches (h)	AC (%)	DSC[b]				
		T_o (°C)	T_p (°C)	T_c (°C)	ΔT (°C)	ΔH (J/g)
0	26.1 ± 0.5f	60.0 ± 0.1c	64.5 ± 0.1a	70.9 ± 0.1a	10.9 ± 0.0a	12.8 ± 0.3e
4	19.2 ± 0.6e	67.5 ± 0.1f	71.7 ± 0.1e	78.1 ± 0.4c	10.6 ± 0.3a	13.0 ± 0.2e
8	15.3 ± 0.7d	66.0 ± 0.0e	72.3 ± 0.0f	79.9 ± 0.1d	13.9 ± 0.1b	8.0 ± 0.3d
12	9.6 ± 0.7c	61.6 ± 0.1d	71.3 ± 0.0d	78.9 ± 0.1c	17.3 ± 0.0c	5.9 ± 0.1c
16	7.3 ± 0.7b	59.1 ± 0.2b	70.7 ± 0.0c	78.5 ± 0.2c	19.4 ± 0.4d	4.8 ± 0.3b
24	0.6 ± 0.7a	56.5 ± 0.3a	70.0 ± 0.1b	76.0 ± 0.0b	19.5 ± 0.3d	2.1 ± 0.1a
36	0.1 ± 0.1a	58.6 ± 0.1b	70.2 ± 0.1b	87.1 ± 0.4e	28.6 ± 0.4e	1.9 ± 0.3a

[a] Data (Mean ± SD) in the same column with different letters were significantly different ($n = 3$ for AC and 2 for DSC, $p < 0.05$).
[b] T_o, onset temperature; T_p, peak temperature; T_c, conclusion temperature; ΔT, gelatinization transition range (T_c–T_o); ΔH, enthalpy of gelatinization.

3.7. SAXS spectra of acid-modified starch

The semicrystalline layers of starch granules consist of a lamellar arrangement of crystalline and amorphous regions with repeat distance of 90–100 Å that is readily detected in hydrated starch by SAXS (Blazek & Gilbert, 2011). The well-resolved main scattering peak around scattering vector of about 0.06 $Å^{-1}$ is thought to arise from the periodic arrangement of alternating crystalline and amorphous lamellae of amylopectin and corresponds to lamellar repeat distance or Bragg spacing. The location of the peak depends on the size of lamella, and may differ for starch originated from different plants, while the peak area or intensity depends mainly on the degree of ordering in semicrystalline regions (Blazek & Gilbert, 2011; Pikus, 2005). The parameters of the SAXS peak can be determined by the simple graphical method (Fig. 5A; Yuryev et al., 2004). The Bragg spacing D can be calculated from the position of the peak (S_{max}) according to $D = 2\pi/S_{max}$.

The SAXS patterns of acid-modified lotus starches are shown in Fig. 5B. All starches were scaled to equal intensity at high q ($q = 0.2$ $Å^{-1}$) to account for variations in sample concentration (Sanderson, Daniels, Donald, Blennow, & Engelsen, 2006). The SAXS patterns were at the same relative scale and therefore directly comparable. The SAXS-derived parameters of acid-modified starch according to Fig. 5A are presented in Table 1. It was evident from Fig. 5B and Table 1 that the diffraction peak position and Bragg spacing were approximately constant, and the ΔS slightly decreased during hydrolysis. The peak intensity increased significantly during the first 4 h of acid hydrolysis and then increased at a slower rate between 4 and 12 h of hydrolysis. After 12 h of hydrolysis, peak intensity gradually decreased to the point when it was barely evident after 48 h of hydrolysis. The present results for the changes in SAXS patterns were in general agreement with data published by Wang et al. (2012) who showed that the lamellar peak intensity increased during early stages of acid hydrolysis, followed by a decrease in the later stages of hydrolysis. The increase in peak intensity could arise from the degradation of the amorphous growth rings or amorphous lamellae with the latter also giving rise to corresponding increases in the lamellar peak intensity (Blazek & Gilbert, 2011; Wang et al., 2012). Thus, during the initial stage of hydrolysis, the significant increase in relative peak intensity was consistent with a more rapid degradation of amorphous regions, the slow increase corresponded to the hydrolysis of amorphous growth rings and amorphous lamellae, and the decrease at the later stage of hydrolysis was attributed to the hydrolysis of crystalline regions. The changes of peak intensity of SAXS patterns were in agreement with the changes of morphology and birefringence during hydrolysis (Fig. 2).

3.8. Amylose content of acid-modified starch

The apparent amylose contents of acid-modified starches, as measured by iodine binding, are presented in Table 2. A gradual decrease in amylose content was observed with increasing hydrolysis time. After 36 h of hydrolysis, amylose content reduced to approximate zero. An early decrease in amylose content has also been reported during acid hydrolysis (Wang et al., 2012). Amylose is largely located in the amorphous regions (growth rings) of starch granules. Hence, it is plausible to suggest that preferential acid attack in the amorphous regions leads to hydrolysis of amylose, consisted with the observed decrease in amylose content (Wang et al., 2012).

3.9. Thermal property of acid-modified starch

Fig. 6 presents the gelatinization thermograms of lotus native and acid-modified starches. The native starch displayed well-defined peaks. There was a progressive reduction of peak height and a broadening of peaks as the time of hydrolysis increased. The

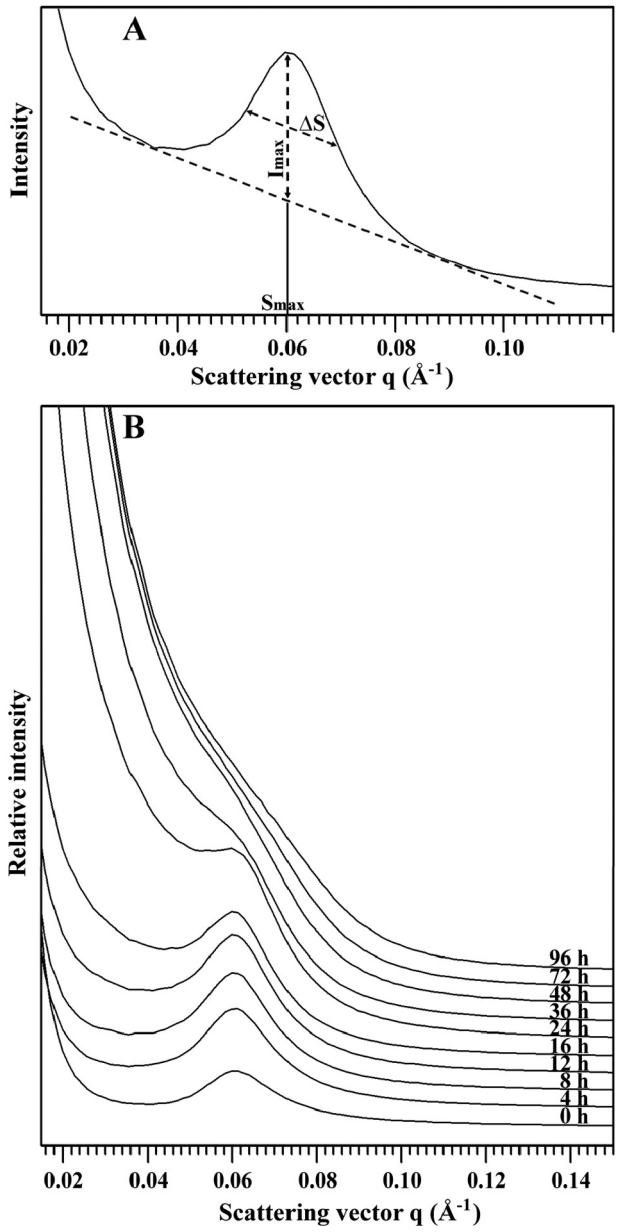

Fig. 5. The sketch of the graphic determination for SAXS parameters (A) and SAXS patterns of acid-modified starches (B). S_{max}, maximum peak position; I_{max}, peak intensity; ΔS, peak full width at half maximum.

changes of thermograms of lotus acid-modified starch were comparable with other acid-modified starches (Campanha & Franco, 2011; Jacobs et al., 1998; Thirathumthavorn & Charoenrein, 2005). After 36 h of hydrolysis, the endothermal peaks were undefined and could not be integrated to the exact values of gelatinization onset temperature (T_o), peak temperature (T_p), conclusion temperature (T_c) and enthalpy (ΔH). Before 36 h of hydrolysis, the thermal parameters of acid-modified starches are given in Table 2. T_o significantly increased at 4 h of hydrolysis, then gradually decreased with increasing hydrolysis time. T_p and T_c significantly increased after 4 h of hydrolysis. However, no further increase in T_p and T_c was observed after 8 h of hydrolysis. Gelatinization transition range (ΔT) gradually increased and ΔH decreased after 8 h of hydrolysis. Similar changes of thermal parameters as a result of acid hydrolysis were observed before for native wheat, rice, pea, potato, and cassava starches (Campanha & Franco, 2011; Jacobs et al., 1998; Thirathumthavorn & Charoenrein, 2005).

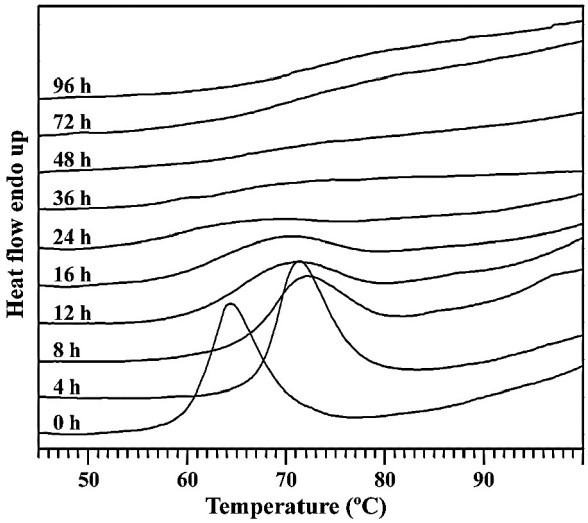

Fig. 6. DSC thermograms of acid-modified starches.

In excess water, the amorphous parts in starch granules exert a destabilizing effect on the crystallites by absorption of water and subsequent swelling because of covalent coupling between amorphous and crystalline parts. Since acid hydrolysis preferentially attacks the amorphous regions in the granule, the crystallites are decoupled from and no longer destabilized by the amorphous parts. As a result, the crystallites melt at a higher temperature and the transition is broader, indicating the heterogeneous distribution in crystallite stability in the starch granule (Jacobs et al., 1998). A reduction in the enthalpy of gelatinization occurs because acid primarily attacks the amorphous regions in the granules and these regions play an important role in the thermodynamics of gelatinization (Thirathumthavorn & Charoenrein, 2005).

3.10. Allomorph distribution in lotus rhizome C-type starch granule

According to the changes of morphologies of lotus acid-modified starches, starch granule could be categorized into three parts. The first part was the region located on the end of granule opposite to the eccentric hilum, the second part was the central area, and the third part was the periphery of hilum. The hydrolysis of granule began from the first part, then propagated into the second part, accompanied by loss of birefringence. The third part was most resistant to hydrolysis. Starch crystallinity changed from C-type to A-type via C_A-type during hydrolysis. Therefore, the first part was mainly the B-type allomorph, the second part mainly consisted of A- and B-type allomorphs, and the third part was mainly the A-type allomorph. This allomorph distribution of lotus C-type starch was never reported, which was different from that of pea C-type starch with B-type allomorph around the central hilum and A-type allomorph at the granule periphery (Bogracheva et al., 1998; Buléon et al., 1998).

C-type starch consists of A- and B-type allomorphs (Bogracheva et al., 1998; Cheetham & Tao, 1998; Wang et al., 2009). If the A- and B-type allomorphs are distributed in different granules, then it is likely that the properties of C-type starches would be intermediate between those of A- and B-type starches. If, on the other hand, the A- and B-type allomorphs exist within the same granules, then C-type starches would have unique properties dependent upon the arrangement of those two allomorphs in the granule (Bogracheva et al., 1998; Wang et al., 2009). For pea and high-amylose rice TRS C-type starches, the A- and B-type allomorphs exist within the same granules, but their distributions are significantly different, which

results in different functional properties and applications in food and nonfood industries (Bogracheva et al., 1998; Man, Qin, et al., 2012; Wang et al., 2012; Wei, Qin, et al., 2010; Wei, Xu, et al., 2010; Wei et al., 2011). The present results showed that the arrangement of A- and B-type allomorphs in lotus rhizome starch was different from that in pea and TRS starches, and would affect the functional properties and applications of lotus rhizome starch in food and nonfood industries.

4. Conclusion

Lotus rhizome starch had the eccentric hilum, showed C-type crystallinity containing A- and B-type allomorphs. The degradation of granule during hydrolysis began from the end distant from the hilum and then propagated into the center of granule, accompanied by loss of birefringence. The periphery region of hilum end was more resistant to hydrolysis and had birefringence at the last stage of hydrolysis. The crystallinity changed from C-type to A-type via C_A-type during hydrolysis. At the early stage of hydrolysis, the amylose content substantially reduced, the peak and conclusion gelatinization temperatures increased, and the enthalpy decreased. During hydrolysis, the relative double helix content gradually increased and the amorphous component decreased, the lamellar peak intensity firstly increased and then decreased accompanied by hydrolysis of amorphous and crystalline regions. The changes of morphology and spectrum of acid-modified starches indicated that B-type allomorph was mainly arranged in the distal region of the eccentric hilum, A-type allomorph was mainly located in the periphery region of hilum end, and the center of the granule was a mixed distribution of A- and B-type allomorphs.

Acknowledgements

This study was financially supported by grants from the National Natural Science Foundation of China (31071342, 31270221), the Talent Project of Yangzhou University, and the Priority Academic Program Development from Jiangsu Government, China.

References

Atichokudomchai, N., Varavinit, S., & Chinachoti, P. (2004). A study of ordered structure in acid-modified tapioca starch by ^{13}C CP/MAS solid-state NMR. *Carbohydrate Polymers*, *58*, 383–389.

Blazek, J., & Gilbert, E. P. (2011). Application of small-angle X-ray and neutron scattering techniques to the characterisation of starch structure: A review. *Carbohydrate Polymers*, *85*, 281–293.

Bogracheva, T. Y., Morris, V. J., Ring, S. G., & Hedley, C. L. (1998). The granular structure of C-type pea starch and its role in gelatinization. *Biopolymers*, *45*, 323–332.

Bogracheva, T. Y., Wang, Y. L., & Hedley, C. L. (2001). The effect of water content on the ordered/disordered structures in starches. *Biopolymers*, *58*, 247–259.

Buléon, A., Gérard, C., Riekel, C., Vuong, R., & Chanzy, H. (1998). Details of the crystalline ultrastructure of C-starch granules revealed by synchrotron microfocus mapping. *Macromolecules*, *31*, 6605–6610.

Campanha, R. B., & Franco, C. M. L. (2011). Gelatinization properties of native starches and their Nägeli dextrins. *Journal of Thermal Analysis and Calorimetry*, *106*, 799–804.

Cheetham, N. W. H., & Tao, L. (1998). Variation in crystalline type with amylose content in maize starch granules: An X-ray powder diffraction study. *Carbohydrate Polymers*, *36*, 277–284.

Chung, Y. L., & Lai, H. M. (2006). Molecular and granular characteristics of corn starch modified by HCl–methanol at different temperatures. *Carbohydrate Polymers*, *63*, 527–534.

Htoon, A., Shrestha, A. K., Flanagan, B. M., Lopez-Rubio, A., Bird, A. R., Gilbert, E. P., et al. (2009). Effects of processing high amylose maize starches under controlled conditions on structural organisation and amylase digestibility. *Carbohydrate Polymers*, *75*, 236–245.

Jacobs, H., Eerlingen, R. C., Rouseu, N., Colonna, P., & Delcour, J. A. (1998). Acid hydrolysis of native and annealed wheat, potato and pea starches – DSC melting features and chain length distributions of lintnerised starches. *Carbohydrate Research*, *308*, 359–371.

Konik-Rose, C., Thistleton, J., Chanvrier, H., Tan, I., Halley, P., Gidley, M., et al. (2007). Effects of starch synthase IIa gene dosage on grain, protein and starch in endosperm of wheat. *Theoretical and Applied Genetics*, *115*, 1053–1065.

Li, W., Corke, H., & Beta, T. (2007). Kinetics of hydrolysis and changes in amylose content during preparation of microcrystalline starch from high-amylose maize starches. *Carbohydrate Polymers*, *69*, 398–405.

Lin, H. M., Chang, Y. H., Lin, J. H., Jane, J. L., Sheu, M. J., & Lu, T. J. (2006). Heterogeneity of lotus rhizome starch granules as revealed by α-amylase degradation. *Carbohydrate Polymers*, *66*, 528–536.

Man, J. M., Cai, J. W., Cai, C. H., Xu, B., Huai, H. Y., & Wei, C. X. (2012). Comparison of physicochemical properties of starches from seed and rhizome of lotus. *Carbohydrate Polymers*, *88*, 676–683.

Man, J. M., Qin, F. L., Zhu, L. J., Shi, Y. C., Gu, M. H., Liu, Q. Q., et al. (2012). Ordered structure and thermal property of acid-modified high-amylose rice starch. *Food Chemistry*, *134*, 2242–2248.

Pérez, S., Baldwin, P. M., & Gallant, D. J. (2009). Structural features of starch granules I. In J. BeMiller, & R. Whistler (Eds.), *Starch: Chemistry and technology* (3rd ed., pp. 149–192). Amsterdam: Academic Press.

Pikus, S. (2005). Small-angle X-ray scattering studies of the structure of starch and starch products. *Fibres and Textiles in Eastern Europe*, *13*, 82–86.

Sanderson, J. S., Daniels, R. D., Donald, A. M., Blennow, A., & Engelsen, S. B. (2006). Exploratory SAXS and HPAEC-PAD studies of starches from diverse plant genotypes. *Carbohydrate Polymers*, *64*, 433–443.

Sevenou, O., Hill, S. E., Farhat, I. A., & Mitchell, J. R. (2002). Organisation of the external region of the starch granule as determined by infrared spectroscopy. *International Journal of Biological Macromolecules*, *31*, 79–85.

Tan, I., Flanagan, B. M., Halley, P. J., Whittaker, A. K., & Gidley, M. J. (2007). A method for estimating the nature and relative proportions of amorphous, single, and double-helical components in starch granules by ^{13}C CP/MAS NMR. *Biomacromolecules*, *8*, 885–891.

Thirathumthavorn, D., & Charoenrein, S. (2005). Thermal and pasting properties of acid-treated rice starches. *Starch*, *57*, 217–222.

Wang, L. F., & Wang, Y. J. (2001). Structures and physicochemical properties of acid-thinned corn, potato and rice starches. *Starch*, *53*, 570–576.

Wang, S. J., Blazek, J., Gilbert, E., & Copeland, L. (2012). New insights on the mechanism of acid degradation of pea starch. *Carbohydrate Polymers*, *87*, 1941–1949.

Wang, S. J., Yu, J. L., Zhu, Q. H., Yu, J. G., & Jin, F. M. (2009). Granular structure and allomorph position in C-type Chinese yam starch granule revealed by SEM, ^{13}C CP/MAS NMR and XRD. *Food Hydrocolloids*, *23*, 426–433.

Wang, S. J., Yu, J. L., Yu, J. G., Chen, H. X., & Pang, J. P. (2007). The effect of acid hydrolysis on morphological and crystalline properties of Rhizome *Dioscorea* starch. *Food Hydrocolloids*, *21*, 1217–1222.

Wei, C. X., Qin, F. L., Zhou, W. D., Xu, B., Chen, C., Chen, Y. F., et al. (2011). Comparison of the crystalline properties and structural changes of starches from high-amylose transgenic rice and its wild type during heating. *Food Chemistry*, *128*, 645–652.

Wei, C. X., Qin, F. L., Zhou, W. D., Yu, H. G., Xu, B., Chen, C., et al. (2010). Granule structure and distribution of allomorphs in C-type high-amylose rice starch granule modified by antisense RNA inhibition of starch branching enzyme. *Journal of Agricultural and Food Chemistry*, *58*, 11946–11954.

Wei, C. X., Xu, B., Qin, F. L., Yu, H. G., Chen, C., Meng, X. L., et al. (2010). C-type starch from high-amylose rice resistant starch granules modified by antisense RNA inhibition of starch branching enzyme. *Journal of Agricultural and Food Chemistry*, *58*, 7383–7388.

Yuryev, V. P., Krivandin, A. V., Kiseleva, V. I., Wasserman, L. A., Genkina, N. K., Fornal, J., et al. (2004). Structural parameters of amylopectin clusters and semi-crystalline growth rings in wheat starches with different amylose content. *Carbohydrate Research*, *339*, 2683–2691.